

This discussion paper is/has been under review for the journal Atmospheric Chemistry and Physics (ACP). Please refer to the corresponding final paper in ACP if available.

# A map of radon flux at the Australian land surface

**A. D. Griffiths, W. Zahorowski, A. Element, and S. Werczynski**

Australian Nuclear Science and Technology Organisation, Locked Bag 2001, Kirrawee DC, NSW, 2232, Australia

Received: 27 April 2010 – Accepted: 28 May 2010 – Published: 9 June 2010

Correspondence to: A. D. Griffiths (alan.griffiths@ansto.gov.au)

Published by Copernicus Publications on behalf of the European Geosciences Union.

## A map of radon flux at the Australian land surface

A. D. Griffiths et al.

Title Page

Abstract

Introduction

Conclusions

References

Tables

Figures

◀

▶

◀

▶

Back

Close

Full Screen / Esc

Printer-friendly Version

Interactive Discussion



## Abstract

A time-dependent map of radon-222 flux density at the Australian land surface has been constructed with a spatial resolution of  $0.05^\circ$  and temporal resolution of one month. Radon flux density was calculated from a simple model utilising data from national gamma-ray aerial surveys, modelled soil moisture, and maps of soil properties. The model was calibrated against a large data set of accumulation-chamber measurements, thereby constraining it with experimental data. A notable application of the map is in atmospheric mixing and transport studies which use radon as a tracer, where it is a clear improvement on the common assumption of uniform radon flux density.

## 1 Introduction

Radon-222, or radon, is a radioactive noble gas which is exhaled by soil and rock to the atmosphere. Radioactive decay is the only significant removal process, so it is an ideal tracer for studying physical processes with a timescale comparable to its 3.8 day half-life.

Radon-222 is a member of the uranium-238 decay series and its immediate parent is radium-226, with a half-life of 1600 years. Radon-222 decays to polonium-218 (half-life of 3.1 min) followed by lead-214 (half-life of 27 min) and then to bismuth-214.

Bismuth-214 is the first element in the series which emits gamma rays that can be detected in aerial surveys. By assuming secular equilibrium, data from these surveys can be used to map the topsoil concentration of radioelements in the uranium-238 decay series (Minty, 1997).

Radon-220, or thoron, is a less abundant radon isotope and a member of the thorium-232 decay series. With a half-life of 56 s, it is suited to studying vertical mixing in the atmospheric surface layer (Lehmann et al., 1999). A gamma emitter in the thorium decay series, thallium-208, can be used to map the concentration of radioisotopes in the thorium series, so the methods used to map radon-222 fluxes can be similarly

## A map of radon flux at the Australian land surface

A. D. Griffiths et al.

Title Page

Abstract

Introduction

Conclusions

References

Tables

Figures



Back

Close

Full Screen / Esc

Printer-friendly Version

Interactive Discussion



applied to radon-220. In this paper, however, we consider radon-220 only as an aid in interpreting our results.

Globally, the land surface is the dominant source of radon, the flux density at the ocean surface being around two orders of magnitude smaller (Schery and Huang, 2004). Although commonly assumed to be constant, the land-surface flux of radon varies in space and time. The constant-flux assumption is convenient because the global mean radon flux density has been well known for some time (e.g. Jacob et al., 1997) whereas variations on smaller scales are not well characterised.

Uncertainty in flux density limits the usefulness of radon in atmospheric studies, where it has found numerous applications. These include using radon to test mixing and transport processes in atmospheric models (Gupta et al., 2004; Jacob et al., 1997; Zhang et al., 2008) and for calibrating regional flux estimates of greenhouse gases (Hirsch, 2007; Biraud et al., 2000). These applications, and others, are reviewed by Zahorowski et al. (2004).

Motivated by improving these types of studies, several groups have progressed towards better characterisation of regional radon flux density.

For the northern hemisphere, Conen and Robertson (2002) suggest a radon flux of  $21.0 \text{ mBq m}^2 \text{ s}^{-1}$  ( $1 \text{ atom cm}^{-2} \text{ s}^{-1}$ ) over ice-free land areas south of  $30^\circ \text{ N}$  and a linear decrease northwards to reach of  $4.2 \text{ mBq m}^2 \text{ s}^{-1}$  ( $0.2 \text{ atom cm}^{-2} \text{ s}^{-1}$ ) at  $70^\circ \text{ N}$ . A similar meridional flux density gradient was recently reported by Williams et al. (2009), based on atmospheric measurements in East Asia.

A more detailed map, which includes spatial and temporal variability and yet remains consistent with Conen and Robertson's estimate, has been produced for Europe using gamma dose rate as a proxy (Szegvary et al., 2007, 2009).

For China, a similar map was reported by Zhuo et al. (2008) using a different approach. In the absence of western Europe's high-density gamma dose rate network, Zhuo et al. relied on soil and climate maps to estimate fluxes.

Global maps have also been produced, but their authors point to the maps' preliminary nature (Schery and Wasiolek, 1998) or to the need for better input data (Goto

## A map of radon flux at the Australian land surface

A. D. Griffiths et al.

Title Page

Abstract

Introduction

Conclusions

References

Tables

Figures

◀

▶

◀

▶

Back

Close

Full Screen / Esc

Printer-friendly Version

Interactive Discussion



et al., 2008).

In consequence, the Australian region remains without detailed coverage. The aim of the present work is to develop a map of radon-222 surface flux density covering Australia with a spatial resolution of  $0.05^\circ$  and temporal resolution of one month.

## 2 Methods

In general terms, our approach is to use point measurements of radon flux density to calibrate a simple diffusive transport model and then use the model to generate a map.

We restrict ourselves to a simple model, even though more sophisticated models are required to better reproduce day-to-day variations in radon flux (Holford et al., 1993).

This is because input parameters are available to drive a simple model at regional scale and because, over time periods of about ten days or longer, the mean flux density is close to that calculated from diffusion (Schery et al., 1984). Neglecting short-term variability, though, means that instantaneous fluxes may differ from modelled fluxes by around a factor of two (Holford et al., 1993).

### 2.1 Accumulation chamber measurements

The accumulation chamber measurements available for model calibration are listed in Table 1.

At each measurement site, an accumulation chamber was placed on the ground, sealed, and air was drawn from the chamber into two scintillation cells, separated by a six-minute delay line, and back into the chamber. Fluxes of both radon-222 and radon-220 are measured using this approach. Details of the instrument design and data analysis are given in Zahorowski and Whittlestone (1996); for a radon-222 flux of  $4 \text{ mBq m}^{-2} \text{ s}^{-1}$  the counting error is 30% for the 24 min counting period employed here.

This instrument was used to collect all of the data listed in Table 1 with the exception of the mainland survey (Schery et al., 1989). In a comparison with eight others at a

## A map of radon flux at the Australian land surface

A. D. Griffiths et al.

Title Page

Abstract

Introduction

Conclusions

References

Tables

Figures

◀

▶

◀

▶

Back

Close

Full Screen / Esc

Printer-friendly Version

Interactive Discussion



field site, the radon flux density measured with this instrument was within one standard deviation of the mean and higher by 31% (Hutter and Knutson, 1998). More recently, however, the instrument was found to be within 5% of the accumulation chamber used by Szegvary et al. (2007) in a laboratory comparison (Werczynski et al., 2010).

As with all such measurements, the presence of an accumulation chamber reduces the rate at which radon diffuses out of soil, thus introducing a systematic error. Mayya (2004) analysed this effect in a two-dimensional framework and, based on this analysis, our accumulation chamber measurements are expected to be low by about 10%, for a 24 min counting period and assuming soil porosity of  $\epsilon = 0.4$  and radon diffusion length  $l_d = 1$  m (Mayya, 2004, Eq. 26b). A detailed correction for this effect requires knowledge of soil parameters at each measurement site and assumes an idealised accumulation chamber configuration that is not typically realised in the field. As a result, we have chosen to present the flux measurements without this correction and simply note the possibility of a systematic error of around 10% in the final result.

## 2.2 Diffusion model

The transport of radon from soil to air is reviewed by Nazaroff (1992) and here we discuss the simplified representation of this process implemented in our model.

Radon-222 is produced within soil grains at a rate equal to the specific activity of its parent, radium-226. A fraction of the generated radon enters the pore space; this is called the emanation fraction,  $f$ , with a representative range of 0.1–0.4 (Markkanen and Arvela, 1992). The emanation fraction for a dry soil is a factor of 2–3 lower than for soil at around 10% of saturation (Zhuo et al., 2006) because soil grains in moist soil are enveloped by a water film which decelerates recoiling nuclei that would otherwise travel across the pore space to become embedded in adjacent soil grains (Sasaki et al., 2004; Sakoda et al., 2010). Increasing soil moisture beyond 10% has little further impact on  $f$ .

Radon in the air-filled pore space diffuses down the concentration gradient towards the surface. It also diffuses through water, but we neglect this effect as the diffusion

## A map of radon flux at the Australian land surface

A. D. Griffiths et al.

Title Page

Abstract

Introduction

Conclusions

References

Tables

Figures

◀

▶

◀

▶

Back

Close

Full Screen / Esc

Printer-friendly Version

Interactive Discussion



coefficient in water is about five orders of magnitude smaller than in air. For one-dimensional diffusion, the bulk flux density,  $J$ , can be expressed with Flick's law as

$$J = -\epsilon D_e \frac{\partial C}{\partial z}, \quad (1)$$

where  $\epsilon$  is the soil porosity,  $D_e$  is the effective diffusion coefficient in the porous medium and  $C$  is the radon activity concentration in the pore air. As conventions vary, we emphasise that here  $J$  is the flux density per unit bulk area whereas  $C$  is the concentration of radon per unit pore volume. The transport equation for pore-gas radon concentration is derived using (1) assuming conservation of radon, assuming that  $\epsilon$  and  $D_e$  are constants, and including sink and source terms. After these steps

$$\frac{\partial C}{\partial t} = D_e \frac{\partial^2 C}{\partial z^2} - \lambda C + \frac{\lambda \rho_b A_{\text{Ra}} f}{\epsilon} \quad (2)$$

where  $\lambda \simeq 2.1 \times 10^{-6} \text{ s}^{-1}$  is the radon-222 decay constant,  $A_{\text{Ra}}$  is the specific activity of radium-226 (units of activity per mass of dry soil) and  $\rho_b$  is the dry soil bulk density.

To solve Eq. (2) we assume: steady-state; the existence of a soil layer of infinite thickness with soil-air interface at  $z = 0$ ; a coordinate system with positive  $z$  downwards; and boundary conditions  $C(0) = 0$  and finite  $C(\infty)$ . Choosing  $C(0) = 0$  is generally a good approximation as atmospheric radon concentrations are typically three orders of magnitude smaller than in the soil gas at depth. With these boundary conditions

$$C = C_\infty [1 - \exp(-z/l_d)], \quad (3)$$

where  $C_\infty = \rho_b A_{\text{Ra}} f / \epsilon$  is the asymptotic radon concentration at depth and  $l_d = \sqrt{D_e / \lambda}$  is called the diffusion length, the characteristic length that radon atoms diffuse before decaying. By evaluating  $\partial C / \partial z$  at  $z = 0$  and substituting into Eq. (1) we find that the flux density at the surface is

$$J(0) = -\rho_b A_{\text{Ra}} f \sqrt{\lambda D_e}, \quad (4)$$

**A map of radon flux at the Australian land surface**

A. D. Griffiths et al.

Title Page

Abstract

Introduction

Conclusions

References

Tables

Figures

⏪

⏩

◀

▶

Back

Close

Full Screen / Esc

Printer-friendly Version

Interactive Discussion



which is negative signifying radon transport from soil to air.

Having defined  $l_d$ , we can relax the need for an infinitely thick soil layer, and instead require a layer of thickness  $d \gg l_d$ . For radon-222,  $l_d \sim 1$  m is typical so  $d \gg l_d$  is not necessarily realised in practise.

5 Empirical relationships are used to define  $f$  and  $D_e$ . Following Zhuo et al. (2008), the emanation fraction is

$$f = f_0 \{1 + a[1 - \exp(-bm)]\} [1 + c(T - 298)] \quad (5)$$

where  $f_0$ ,  $a$ ,  $b$  and  $c$  are parameters (shown in Table 2) that depend on soil texture, and  $T$  is soil temperature in kelvin. By defining a general soil as a mixture of clay, silt  
10 and sand, we compute  $f$  as a weighted sum according to the fraction of each texture class.

The effective diffusion coefficient,  $D_e$ , is defined according to an observed correlation with soil moisture (Rogers and Nielson, 1991),

$$D_e = D_{a0} \epsilon \exp(-6m\epsilon - 6m^{14\epsilon}) \quad (6)$$

15 where  $D_{a0} = 1.1 \times 10^{-5} \text{m}^2 \text{s}^{-1}$  is the diffusion coefficient for radon in air,  $m$  is moisture saturation with  $0 \leq m \leq 1$ , and  $\epsilon$  is porosity.

Both  $f$  and  $D_e$  are functions of moisture, so flux density at the soil surface is a nonlinear function of moisture with a maximum around  $m = 0.1$  (Fig. 1).

This model can be extended by defining two layers of homogeneous soil. Layer 1  
20 extends from the surface to an arbitrary depth  $d_1$ , and layer 2 extends from  $d_1$  down to  $d_2 = \infty$ , though physically we take this to mean that  $d_2 - d_1 \gg l_d$ . Soil properties, including moisture, are constant within layers but are permitted to take different values in each layer and are assigned the subscript 1 or 2 to indicate which layer they apply to.

25 As before,  $C(0) = 0$  and  $C(\infty)$  is finite. In addition,  $C$  and  $J$  are continuous at  $d_1$ , the interface between the layers.

## A map of radon flux at the Australian land surface

A. D. Griffiths et al.

Title Page

Abstract

Introduction

Conclusions

References

Tables

Figures

◀

▶

◀

▶

Back

Close

Full Screen / Esc

Printer-friendly Version

Interactive Discussion



The steady state solution can be expressed analytically. At the soil surface, the flux density is

$$J(0) = \frac{\left[2f_1 B \sqrt{D_{e1}}\right] J_{02} + \left[f_2(B-1)^2 \sqrt{D_{e2}} + f_1(1-B^2) \sqrt{D_{e1}}\right] J_{01}}{f_2(1-B^2) \sqrt{D_{e2}} + f_1(B^2+1) \sqrt{D_{e1}}} \quad (7)$$

where

$$J_{01} = -\rho_1 A_{Ra1} f_1 \sqrt{\lambda D_{e1}} \quad (8)$$

$$J_{02} = -\rho_2 A_{Ra2} f_2 \sqrt{\lambda D_{e2}} \quad (9)$$

$$B = \exp\left(-d_1 \sqrt{\lambda/D_{e1}}\right) = \exp(-d_1/l_{d1}) \quad (10)$$

The terms  $J_{01}$  and  $J_{02}$  are surface fluxes that would be observed for homogeneous soil with the properties of layer 1 or 2, whereas  $B$  depends on the ratio of the interface depth to the diffusion length in the top layer.

Compared with the single-layer expression, Eq. (4), the two-layer expression can represent situations where a nearly-saturated surface layer blocks radon transport to the surface even if the soil below is dry. The model could be extended further with additional soil layers; we use two layers because this matches the definition of the input data.

During production of the map, radon flux density estimates calculated from Eq. (7), which we here denote as  $J'$ , were converted to calibrated estimates,  $J_c$ , where

$$J_c = cJ' \quad (11)$$

and  $c$  is the calibration factor, which is assumed to be constant. Flux chamber measurements were used to find  $c$  by minimising the difference between  $J_c$  and measured

**A map of radon flux at the Australian land surface**

A. D. Griffiths et al.

Discussion Paper | Discussion Paper | Discussion Paper | Discussion Paper | Discussion Paper

Title Page

Abstract

Introduction

Conclusions

References

Tables

Figures

◀

▶

◀

▶

Back

Close

Full Screen / Esc

Printer-friendly Version

Interactive Discussion



fluxes in log space. This is equivalent to finding  $c$  such that

$$c = \left( \prod_{i=1}^N \frac{J_i}{J'_i} \right)^{\frac{1}{N}} \quad (12)$$

where  $J_i$  is the measured flux at the  $i$ th measurement location and  $J'_i$  is the uncalibrated modelled flux at the  $i$ th measurement location.

By minimising the error in log space, the computed value of  $c$  is sensitive to data from locations with both large and small flux density, which is desirable as large radon fluxes are not distributed evenly throughout the measurement set.

### 2.3 Model input data

The soil properties required to evaluate Eq. (7) are: radium specific activity,  $A_{\text{Ra}}$ , moisture,  $m$ , bulk density,  $\rho_b$ , porosity,  $\epsilon$ , and soil texture expressed as the fraction of clay, silt and sand. Radium data are taken from the Radiometric Map of Australia (Radmap 2009: Minty et al., 2009), and topsoil and subsoil moisture from the Australian Water Availability Project (AWAP: Raupach et al., 2008, 2009). Other soil properties originate from interpretations of the Atlas of Australian Soils (Northcote et al., 1960; McKenzie and Hook, 1992; McKenzie et al., 2000), which we obtained in digital form from the AWAP model and the Australian Natural Resources Data Library website (Bureau of Rural Sciences, 2009).

Radmap 2009 is a mosaic of individual gamma ray aerial surveys (Minty, 2000), mostly with flight-line spacing of 500 m or less. It is back-calibrated to a coarse grid, flown in March–December 2007, covering the country with flight line spacing of 75 km and which is itself back-calibrated to the IAEA global datum.

Radmap coverage is close to 90% of the land mass, as shown in Fig. 2. To obtain a complete map, soil radium in areas without coverage was estimated by natural neighbour interpolation (Watson, 1999) to arrive at the distribution shown in Fig. 3.

## A map of radon flux at the Australian land surface

A. D. Griffiths et al.

Title Page

Abstract

Introduction

Conclusions

References

Tables

Figures



Back

Close

Full Screen / Esc

Printer-friendly Version

Interactive Discussion



Although the gamma-ray signal comes from roughly the top 20 cm of soil, we assume that soil radium content is invariant with depth.

Soil moisture is an important factor controlling flux density and, as modelled in this paper, is the only time-varying model input. As the diffusion length of radon-222 is large enough for the surface flux to be influenced by subsoil moisture, it is desirable to include this parameter in the flux model.

The AWAP model simulates soil moisture in a topsoil and subsoil layer with thicknesses defined from the Atlas of Australian Soils. The mean topsoil thickness is 23 cm and the mean subsoil thickness is 59 cm. To calculate flux density, soil below the subsoil layer is assumed to have the same properties as the subsoil.

Radon flux density is calculated on the same grid as soil moisture, which is the lowest resolution input. This is a  $0.05^\circ$  grid, which equates to approximately  $5 \times 5$  km grid squares.

Other soil properties; bulk density, porosity, and texture; are taken from empirical correlations. These are correlations which have been observed between mapped soil types and soil physical properties (McKenzie and Hook, 1992; McKenzie et al., 2000). As these properties have been arrived at indirectly, there is considerable uncertainty in their derivation and are, according to McKenzie et al. (2000), an 'interim measure' prior to better estimates becoming available. As a result, the spatial variation in flux density that arises from changes in soil properties is expected to be poorly depicted in the model compared with the effect of soil moisture and radium patterns.

### 3 Results

#### 3.1 Accumulation chamber measurements

The results from accumulation chamber measurements are summarised in Table 1. The results are grouped into data sets by measurement campaign: the Tasmania and Mainland data sets are large-area surveys; the Cowra, Mary River and Goulburn sur-

## A map of radon flux at the Australian land surface

A. D. Griffiths et al.

Title Page

Abstract

Introduction

Conclusions

References

Tables

Figures



Back

Close

Full Screen / Esc

Printer-friendly Version

Interactive Discussion



veys cover small areas of less than 40 km across; and the Cataract coverage area was smaller still with 400 m between the furthest points.

### 3.2 Radiometrics versus fluxes

Previous studies have found a correlation between radon flux density and terrestrial gamma dose rate (Schery et al., 1989; Szegvary et al., 2007). A strong correlation may therefore also be expected between flux density and the gamma ray activity arising only from bismuth-214, a decay product of radon-222.

To test this hypothesis, radiometric measurements were made at flux measurement points during the Cowra and Mary River surveys, using an Exploranium GR-320 gamma spectrometer at the former and a Radiation Solutions RS-230 gamma spectrometer at the latter. These instruments rely on the same measurement principle as aerial surveys, but can be located at the same place as the flux measurement. Soil radium can vary significantly over the space of ten metres or less, so co-locating the measurements maximises the chance of observing a correlation between gamma intensity and radon flux density.

This comparison is shown in Fig. 4 for the two areas. Both data sets show higher radon flux density at sites which, based on bismuth-214 activity, have more radium in the soil.

The radiometric signal explains more of the variance in the Cowra data set than the Mary River data, as judged from the  $R^2$  values. This may be explained by less variability in the soil type at Cowra, as was observed qualitatively in the field.

Although a relationship between soil radium and radon flux density is well supported within each of the data sets, the importance of other factors is also revealed. For the same equivalent specific activity of radium, Cowra fluxes are three times larger than at Mary River. In the context of our model, this may be a result of the two areas having different soil types, different soil moisture, or a combination of both.

## A map of radon flux at the Australian land surface

A. D. Griffiths et al.

Title Page

Abstract

Introduction

Conclusions

References

Tables

Figures

◀

▶

◀

▶

Back

Close

Full Screen / Esc

Printer-friendly Version

Interactive Discussion



### 3.3 Modelled versus observed seasonal cycle

Seasonal changes in soil moisture lead to seasonal changes in radon exhalation as very dry soil or very wet soil reduces flux density at the surface.

The Cataract data set, detailed in Table 1, is a year-long time series of radon measurements acquired by sampling seven nearby sites (within 400 m) each fortnight. The temporal changes in radon-222 flux were not well correlated between these sites, though the sites were consistent in the sense that, for most measurements, the ordering of low to high flux remained constant.

Compared with radon-222, variations in radon-220 flux (not shown) were more strongly correlated across sites, perhaps reflecting the topsoil having a more uniform response to precipitation/evaporation than the subsoil.

As our model lacks the spatial resolution to capture the spatial variability between sites, we focus on the temporal evolution of the mean flux across the seven sites, as shown in Fig. 5. The model, uncalibrated, overestimates radon flux density up until May and then follows observations reasonably well, correctly capturing the minimum in late September.

On the other hand, the flux density at this location changes little throughout the year and a constant would fit the observations just as well as the model. Combined with the low signal-to-noise ratio in the data, it appears that this location, at least for 1998, is not a strong test of the model's representation of temporal changes.

Some other, though limited, data exist to which we can compare the model. Whittlestone et al. (1998) attempted to quantify the seasonal variation of radon flux density in Tasmania by making measurements in February and then again in July 1996. Averaged across all sites, the flux density in February,  $31 \text{ mBq m}^{-2} \text{ s}^{-1}$ , was larger than that measured in July,  $15 \text{ mBq m}^{-2} \text{ s}^{-1}$ , by a factor of 2.1. This compares well with the seasonal variation in the model which, averaged across Tasmania, was a factor of 2.4 for the same times.

Not all points were sampled twice by Whittlestone et al., however; a comparison

## A map of radon flux at the Australian land surface

A. D. Griffiths et al.

Title Page

Abstract

Introduction

Conclusions

References

Tables

Figures

◀

▶

◀

▶

Back

Close

Full Screen / Esc

Printer-friendly Version

Interactive Discussion



including only those sites sampled twice, 10 out of a total of 54, shows a smaller seasonal cycle with a ratio of 1.5 between February and July fluxes.

Returning to the data listed in Table 1, the repeat measurements made at Cowra and Goulburn sites are another possible means to examine seasonal variation. Variability in soil moisture is not strongly correlated with seasons at these locations, though, and these data turn out to be poorly suited to validating the moisture effect.

Overall, these data are supportive of the need to include temporal variations in radon flux in the model, which can be achieved by including time-dependant soil moisture. The magnitude of the cycle is not particularly well constrained by these data, though there is a weak indication, from Tasmanian and Cataract data, that the model overestimates the seasonal cycle.

### 3.4 Model calibration

The model was calibrated, according to Eq. (12), from the flux data listed in Table 1 and the result is shown in Fig. 6.

For model calibration the Cataract data were excluded, as were points where either flux density or radium specific activity was 1/10th or less than the Australian average. Cataract data were excluded as these 175 measurements were taken within a small area thus representing only a single soil type and a single pixel of radiometric data, so their inclusion would bias the final result. Low flux points were excluded to prevent the poor signal-to-noise ratio of these points from contributing; for the flux chamber the chosen cut-off corresponds to a relative error of about 40%.

Overall, we find that measured fluxes are larger than fluxes modelled with Eq. (7). The calibration factor is  $c = 1.62 \pm 0.15$ , where the uncertainty estimate is the RMS deviation from  $c$  of repeated line fits, each with one of the measurement data sets excluded. This results in a larger error estimate than consideration only of the measurement errors and is intended to take into account systematic differences between the data sets.

## A map of radon flux at the Australian land surface

A. D. Griffiths et al.

Title Page

Abstract

Introduction

Conclusions

References

Tables

Figures



Back

Close

Full Screen / Esc

Printer-friendly Version

Interactive Discussion



## 3.5 Radon flux maps

By computing Eq. (7) at each model grid-point and applying the calibration factor,  $c$ , we obtain a monthly radon flux map. Averaging over the period for which moisture data are available, 1900–2008, results in the mean radon flux map shown in Fig. 7.

5 The arithmetic mean flux is  $24.1 \pm 2.2 \text{ mBq m}^{-2} \text{ s}^{-1}$ , with uncertainty arising from the uncertainty in  $c$  but not including the uncertainty due to the accumulation chamber technique, which is about 10% as discussed in Sect. 2.1. This is consistent with an earlier estimate,  $22 \text{ mBq m}^{-2} \text{ s}^{-1}$ , from Schery et al. (1989) which was based on the mainland survey data of Table 1.

10 Regions of high and low radon flux in Fig. 7 largely result from variations in soil radium, though moisture is also important in places. The contrast between the east and west coasts of Tasmania is due to soil moisture, for example.

As well as spatial variability, parts of Australia show large seasonal departures from the long-term mean, as shown in Fig. 8. As expected from the model formulation, the seasonal patterns of radon flux follow moisture. Away from the interior, which has a very weak seasonal cycle, changes of  $\pm 10 \text{ mBq m}^{-2} \text{ s}^{-1}$ , almost half of the annual mean, are common.

## 4 Discussion

### 4.1 Map limitations

20 There are two main features of Fig. 6 that point to limitations in the flux map: (1) flux density measurements are scattered about the line of fit; and (2) data from different measurement sets are biased relative to each other. We discuss each of these issues in turn.

25 Although flux density and radium activity measurements rely on counting radioactive decay, and therefore become increasingly noisy at low levels, other uncertainties

## A map of radon flux at the Australian land surface

A. D. Griffiths et al.

Title Page

Abstract

Introduction

Conclusions

References

Tables

Figures



Back

Close

Full Screen / Esc

Printer-friendly Version

Interactive Discussion



dominate the scatter in Fig. 6, particularly uncertainties in model inputs.

An import model input is soil radium, derived from gamma measurements which varied in quality between data sets. For Mary River and Cowra, point measurements were made in the field, whereas the other data sets used the values extracted from aerial surveys. By using aerial surveys, a sampling error is introduced with magnitude dependent on the heterogeneity of the local radium specific activity and uncertainty in the sampling location. For the Goulburn data set, the location of flux measurements was known to about 10 m, so precision was limited by the 500 m spacing of flight lines. For the remaining surveys, locations are known to about 1 km accuracy.

Also a factor is the uncertainty due to soil types, which are expected to be poorly characterised. This contributes to offsets between the different data sets and also to increased scatter in the large-area surveys which sample multiple soil types.

For the Cowra and Mary River data, which were collected over small enough areas to sample relatively consistent soil types and also included ground-based radiometric data, the dominant source of scatter may well be a result of assuming that point measurements of flux density are representative of the monthly mean. Based on observed short-term fluctuations (Holford et al., 1993), this is estimated to be a random error contributing about a factor of two to the measurement uncertainty and is large enough to be a significant contributor to the scatter across the entire data set.

To better understand the biases present in data from the individual campaigns, we consider the Cowra and Mary River data in more detail. From Fig. 6 it is apparent that, although modelled fluxes at Cowra and Mary River are similar, measured fluxes are significantly different. This may indicate that the model is failing to capture some important difference between the locations. In fact, if the model is tuned to match Cowra data it is 2.4 times too high at Mary River. This is only slightly better than the factor of 2.9 difference, which is observed when applying a direct correlation with radiometrics (Fig. 4). In contrast, Fig. 9 shows a stronger correlation between radon-220 and radiometrics and a smaller systematic difference between the two sites.

Both locations were visited during conditions with similar, low, soil moisture, so the

## A map of radon flux at the Australian land surface

A. D. Griffiths et al.

Title Page

Abstract

Introduction

Conclusions

References

Tables

Figures



Back

Close

Full Screen / Esc

Printer-friendly Version

Interactive Discussion



effect of moisture on transport is an unlikely cause of the inconsistency and other soil properties are more likely to be the cause. For instance, the emanation fraction,  $f$ , is spatially resolved in the model but is estimated from a cascade of empirical correlations, as outlined in Sects. 2.2 and 2.3, with a resulting large uncertainty.

Problems with uncertainties in the emanation fraction are exacerbated by a feedback affecting radiometric measurements. In this method, soil radium is determined by counting gamma rays emitted by bismuth-214, a decay product of radon-222, and by assuming that the decay chain is in secular equilibrium. Equilibrium in soil is unlikely, however, as a fraction of radon escapes from the soil surface thus reducing bismuth-214 activity and the apparent radium content of the soil (Dickson and Scott, 1997; Minty and Wilford, 2004).

To estimate the magnitude of this effect, consider an idealised, though typical, case. Assuming dry, semi-infinite, homogeneous soil, the counts recorded by a ground level gamma detector are (Grasty, 1997)

$$\frac{N}{N_0} = 1 - \mu_g f l_d \log \left( 1 + \frac{1}{\mu_g l_d} \right) \quad (13)$$

where  $N_0$  is the number of counts that would be observed without radon transport,  $\mu_g$  is the gamma-ray attenuation coefficient and  $l_d \equiv \sqrt{D_e/\lambda}$  is the diffusion length. The measured radium specific activity,  $A'_{\text{Ra}}$ , is proportional to the number of counts, so from Eq. (13) we can write

$$A'_{\text{Ra}} = (1 - c_J f) A_{\text{Ra}} \quad (14)$$

where  $A_{\text{Ra}}$  is the true radium specific activity and  $c_J = \mu_g l_d \log [1 + 1/(\mu_g l_d)]$  is the radon flux correction. For a typical dry soil,  $\mu_g = 7.23 \text{ m}^{-1}$ , and  $l_d = 1.1 \text{ m}$  so  $c_J = 0.942$ .

Because the model is calibrated against flux measurements, the spatially-averaged flux estimated from the model is unaffected by Eq. (13). Instead, surface fluxes will be

**A map of radon flux at the Australian land surface**

A. D. Griffiths et al.

Title Page

Abstract

Introduction

Conclusions

References

Tables

Figures

◀

▶

◀

▶

Back

Close

Full Screen / Esc

Printer-friendly Version

Interactive Discussion



underestimated in areas with a larger than average emanation fraction and conversely overestimated in areas with a smaller than average emanation fraction. This implies that the flux density spatial variability, resulting from changes in  $f$ , is underestimated in the final map. In the absence of this effect

$$\frac{\partial J}{\partial f} = \frac{J}{f} \quad (15)$$

but, taking into account Eq. (14),

$$\frac{\partial J_m}{\partial f} = \frac{J_m}{f} \frac{1 - 2c_j f}{1 - c_j f}, \quad (16)$$

where  $J_m$  is the modelled flux density. For a soil with  $f = 0.35$ , which is relatively high but corresponds to silt with  $m = 0.1$  (Zhuo et al., 2008), the model underestimates changes in flux with changes in  $f$  by a factor of 1.97.

A similar argument can be followed to determine the effect of changes in the diffusion length but, from Eq. (13), the apparent radium concentration tends towards an asymptote for  $l_d \gtrsim 0.3$  m. Shorter diffusion lengths than this are expected only in unusual situations, such as when soil approaches saturation, so the effect due to changing emanation fraction dominates.

For the thorium channel, which detects gamma rays emitted by thallium-208,  $\lambda/D \ll 1$  and  $N \simeq N_0$  regardless of  $f$ . As a result, radium-224 measurements are unaffected by changes in  $f$ . Comparing Fig. 4 and Fig. 9, radon-220 fluxes match radiometrics more closely across both locations and radon-222 fluxes indeed differ by around twice as much as radon-220. Emanation coefficients for radon-220 and radon-222 can not be assumed to be similar, though (Greeman and Rose, 1996), so the degree to which this effect alone is responsible for the difference between Cowra and Mary River data can not be ascertained without further investigation.

In general, radon-222 transport is more complicated than radon-220 because of the longer diffusion length and the potential for soil properties to change with depth, which

## A map of radon flux at the Australian land surface

A. D. Griffiths et al.

Title Page

Abstract

Introduction

Conclusions

References

Tables

Figures

◀

▶

◀

▶

Back

Close

Full Screen / Esc

Printer-friendly Version

Interactive Discussion



provides an alternative explanation for the difference between Figs. 4 and 9. Regardless of the details of this specific case, the implication is that spatial variability is underestimated to some degree in the final map.

## 4.2 Future work

The Australian region has only a sparse coverage of radon flux density measurements, so there are opportunities to improve the map by gathering more data. As the map calibration is based entirely on point flux measurements, the addition of different types of radon flux density measurements would be useful both to test and improve the map. In particular, long time series in areas of strong seasonal variability or an independent estimate of the integrated radon flux over an area might improve the map.

Enhancements to the moisture or soil parameter data would likely improve the accuracy of the map and would be simple to incorporate into future revisions.

Finally, a similar map could be produced with modest effort for radon-220, although this would require a data set of surface soil moisture with temporal resolution significantly better than one month.

## 4.3 Implications for atmospheric studies

For studies based on the applications of atmospheric radon, the value of using the present map instead of a constant-flux source function depends on whether or not it would significantly change atmospheric radon concentrations to do so. In either real-world observations or models, this will be the case whenever a measurement footprint covers an area whose radon flux differs from the national mean.

Cases of this are easy to envisage, for example: (1) the nocturnal peak radon concentration in a stable nocturnal boundary layer is directly related to the local flux; (2) seasonal variations away from the dry interior are important over large enough areas to drive seasonal variation in daytime radon concentrations; and (3) the mean flux density variability is spatially coherent over sufficiently large scales for atmospheric radon to

## A map of radon flux at the Australian land surface

A. D. Griffiths et al.

Title Page

Abstract

Introduction

Conclusions

References

Tables

Figures

◀

▶

◀

▶

Back

Close

Full Screen / Esc

Printer-friendly Version

Interactive Discussion



depend on wind direction at many sites, even after the integrating effect of atmospheric mixing. The generality of these cases demonstrates the possibility of significant implications for the full range of atmospheric radon studies discussed in the introduction.

## 5 Conclusions

5 Our main result, the first detailed radon flux map produced for Australia, shows that the usual assumption of constant radon flux is inadequate, whether the assumption be applied spatially or temporally. The mean flux density,  $24.1 \pm 2.2 \text{ mBq m}^{-2} \text{ s}^{-1}$ , however, is consistent with a previous estimate based on limited data (Schery et al., 1989).

10 The spatial variability in our map is likely to be an underestimate of the true variability as a result of using gamma surveys to estimate soil radium content. We show that this is because the assumption of secular equilibrium within the radioactive decay chain results in soil radium values which are dependant on the fraction of radon lost to the atmosphere.

15 The map presented here covers a similar spatial extent to the recently published European map (Szegvary et al., 2009), and cross-comparison of the measurement instruments place the two maps on a common scale.

The application of a monthly radon flux map, such as that produced in our study, will enhance the accuracy and applicability of atmospheric studies using radon as a tracer, including simulations of radon in global and regional models.

20 Digital versions of the map are available from the authors.

25 *Acknowledgements.* We gratefully acknowledge the following contributors: Stephen Schery for making his radon flux measurements available; Brian Minty for supplying gamma-ray aerial survey data (copyright Geoscience Australia, 2003) and providing advice on its interpretation; Stewart Whittlestone, Michael Hyde and Melanie Lautenschlger who performed some of the flux measurements; The Australian Water Availability Project, in particular Peter Briggs, for supplying soil moisture data (copyright CSIRO, 2008 and used under the terms of the Creative Commons Attribution-Share Alike License version 3.0); and Alastair Williams and Scott

### A map of radon flux at the Australian land surface

A. D. Griffiths et al.

Title Page

Abstract

Introduction

Conclusions

References

Tables

Figures

◀

▶

◀

▶

Back

Close

Full Screen / Esc

Printer-friendly Version

Interactive Discussion



## References

- Biraud, S., Ciais, P., Ramonet, M., Simmonds, P., Kazan, V., Monfray, P., O'Doherty, S., Spain, T. G., and Jennings, S. G.: European greenhouse gas emissions estimated from continuous atmospheric measurements and radon 222 at Mace Head, Ireland, *J. Geophys. Res.*, 105(D1), 1351–1366, doi:10.1029/1999JD900821, 2000. 14315
- Bureau of Rural Sciences: Australian Natural Resources Data Library, online available at: <http://adl.brs.gov.au/anrdl/>, last access: 28 October 2009. 14321
- Conen, F. and Robertson, L.: Latitudinal distribution of radon-222 flux from continents, *Tellus B*, 54, 127–133, doi:10.1034/j.1600-0889.2002.00365.x, 2002. 14315
- Dickson, B. L. and Scott, K. M.: Interpretation of aerial gamma-ray surveys – adding the geochemical factors, *AGSO J. Aust. Geol. Geophys.*, 17, 187–200, 1997. 14328
- Goto, M., Moriizumi, J., Yamazawa, H., Iida, T., and Zhuo, W.: Estimation of global radon exhalation rate distribution, in: *The Natural Radiation Environment—8th International Symposium*, edited by: Paschoa, A. S., 169–172, American Institute of Physics, 2008. 14315
- Grasty, R. L.: Radon emanation and soil moisture effects on airborne gamma-ray measurements, *Geophysics*, 62, 1379–1385, doi:10.1190/1.1444242, 1997. 14328
- Greeman, D. J. and Rose, A. W.: Factors controlling the emanation of radon and thoron in soils of the eastern USA, *Chem. Geol.*, 129, 1–14, doi:10.1016/0009-2541(95)00128-X, 1996. 14329
- Gupta, M., Douglass, A. R., Kawa, S., and Pawson, S.: Use of radon for evaluation of atmospheric transport models: sensitivity to emissions, *Tellus B*, 56, 404–412, doi:10.1111/j.1600-0889.2004.00124.x, 2004. 14315
- Hirsch, A. I.: On using radon-222 and CO<sub>2</sub> to calculate regional-scale CO<sub>2</sub> fluxes, *Atmos. Chem. Phys.*, 7, 3737–3747, doi:10.5194/acp-7-3737-2007, 2007. 14315
- Holford, D. J., Schery, S. D., Wilson, J. L., and Phillips, F. M.: Modeling Radon Transport in Dry, Cracked Soil, *J. Geophys. Res.*, 98, 567–580, doi:10.1029/92JB01845, 1993. 14316, 14327
- Hutter, A. R. and Knutson, E. O.: An international intercomparison of soil gas radon and radon exhalation measurements, *Health Phys.*, 74, 108–114, doi:10.1097/00004032-199801000-00014, 1998. 14317

## A map of radon flux at the Australian land surface

A. D. Griffiths et al.

Title Page

Abstract

Introduction

Conclusions

References

Tables

Figures

◀

▶

◀

▶

Back

Close

Full Screen / Esc

Printer-friendly Version

Interactive Discussion



## A map of radon flux at the Australian land surface

A. D. Griffiths et al.

Title Page

Abstract

Introduction

Conclusions

References

Tables

Figures

◀

▶

◀

▶

Back

Close

Full Screen / Esc

Printer-friendly Version

Interactive Discussion



Jacob, D., Prather, M., Rasch, P., Shia, R., Balkanski, Y., Beagley, S., Bergmann, D., Black-  
hear, W., Brown, M., Chiba, M., et al.: Evaluation and intercomparison of global atmospheric  
transport models using  $^{222}\text{Rn}$  and other short-lived tracers, *J. Geophys. Res.*, 102, 5953–  
5970, doi:10.1029/96JD02955, 1997. 14315

5 Lehmann, B. E., Lehmann, M., Neftel, A., Gut, A., and Tarakanov, S. V.: Radon-220 calibration  
of near-surface turbulent gas transport, *Geophys. Res. Lett.*, 26, 607–610, 1999. 14314

Markkanen, M. and Arvela, H.: Radon Emanation from Soils, *Radiat. Prot. Dosim.*, 45, 269–  
272, 1992. 14317

Mayya, Y. S.: Theory of radon exhalation into accumulators placed at the soil-atmosphere  
10 interface, *Radiat Prot Dosimetry*, 111, 305–318, doi:10.1093/rpd/nch346, 2004. 14317

McKenzie, N. and Hook, J.: Interpretations of the Atlas of Australian Soils, CSIRO Division of  
Soils Technical Report, 94, 1992. 14321, 14322

15 McKenzie, N., Land, C., and Water: Estimation of Soil Properties Using the Atlas of Australian  
Soils, Tech. Rep. 11/00, CSIRO, <http://www.clw.csiro.au/publications/technical2000/>, 2000.  
14321, 14322

Minty, B.: Fundamentals of airborne gamma-ray spectrometry, *AGSO J. Aust. Geol. Geophys.*,  
17, 39–50, 1997. 14314

Minty, B.: Automatic merging of gridded airborne gamma-ray spectrometric surveys, *Explor.*  
*Geophys.*, 31, 47–51, doi:10.1071/EG00047, 2000. 14321

20 Minty, B. and Wilford, J.: Radon effects in ground gamma-ray spectrometric surveys, *Explor.*  
*Geophys.*, 35, 312–318, doi:10.1071/EG04312, 2004. 14328

Minty, B. R. S., Franklin, R., Milligan, P. R., Richardson, L. M., and Wilford, J.: The Radiometric  
Map of Australia, in: 20th International Geophysical Conference and Exhibition, Australian  
Society of Exploration Geophysicists, Adelaide, 2009. 14321, 14336

25 Nazarov, W.: Radon transport from soil to air, *Rev. Geophys.*, 30, 137–160, doi:10.1029/  
92RG00055, 1992. 14317

Northcote, K., Beckmann, G., Bettenay, E., Churchward, H., Dijk, D. V., Dimmock, G., Hubble,  
G., Isbell, R., McArthur, W., and Murtha, G.: Atlas of Australian Soils, Sheets 1 to 10, with  
explanatory data, 1960. 14321

30 Raupach, M. R., Briggs, P. R., Haverd, V., King, E. A., Paget, M., and Trudinger, C. M.: Aus-  
tralian Water Availability Project, online available at: <http://www.csiro.au/awap/>, 2008. 14321

Raupach, M. R., Briggs, P. R., Haverd, V., King, E. A., Paget, M., and Trudinger, C. M.: Aus-  
tralian Water Availability Project (AWAP): CSIRO Marine and Atmospheric Research Com-

## A map of radon flux at the Australian land surface

A. D. Griffiths et al.

Title Page

Abstract

Introduction

Conclusions

References

Tables

Figures

◀

▶

◀

▶

Back

Close

Full Screen / Esc

Printer-friendly Version

Interactive Discussion



ponent: Final Report for Phase 3, CAWCR technical report, CSIRO, 2009. 14321

Rogers, V. C. and Nielson, K. K.: Correlations for predicting air permeabilities and  $^{222}\text{Rn}$  diffusion coefficients of soils, *Health Phys.*, 61, 225–230, doi:10.1097/00004032-199108000-00006, 1991. 14319

5 Sakoda, A., Ishimori, Y., Hanamoto, K., Kataoka, T., Kawabe, A., and Yamaoka, K.: Experimental and modeling studies of grain size and moisture content effects on radon emanation, *Radiat. Meas.*, 45, 204–210, doi:10.1016/j.radmeas.2010.01.010, 2010. 14317

Sasaki, T., Gunji, Y., and Okuda, T.: Mathematical modeling of Radon emanation, *J. Nucl. Sci. Tech.*, 41, 142–151, doi:10.3327/jnst.41.142, 2004. 14317

10 Schery, S., Gaeddert, D., and Wilkening, M.: Factors affecting exhalation of radon from a gravelly sandy loam, *J. Geophys. Res.*, 89, 7299–7309, doi:10.1029/JD089iD05p07299, 1984. 14316

Schery, S., Whittlestone, S., Hart, K., and Hill, S.: The flux of radon and thoron from Australian soils, *J. Geophys. Res.*, 94, 8567–8576, doi:10.1029/JD094iD06p08567, 1989. 14316, 14323, 14326, 14331, 14336

15 Schery, S. D. and Huang, S.: An estimate of the global distribution of radon emissions from the ocean, *Geophys. Res. Lett.*, 31, L19104, doi:10.1029/2004GL021051, 2004. 14315

Schery, S. D. and Wasiolek, M. A.: Radon and Thoron in the Human Environment, chap. Modeling Radon Flux from the Earth's Surface, 207–217, World Scientific Publishing, World Scientific Publishing, Singapore, 1998. 14315

20 Szegvary, T., Leuenberger, M. C., and Conen, F.: Predicting terrestrial  $^{222}\text{Rn}$  flux using gamma dose rate as a proxy, *Atmos. Chem. Phys.*, 7, 2789–2795, doi:10.5194/acp-7-2789-2007, 2007. 14315, 14317, 14323

25 Szegvary, T., Conen, F., and Ciais, P.: European  $^{222}\text{Rn}$  inventory for applied atmospheric studies, *Atmos. Environ.*, 43, 1536–1539, doi:10.1016/j.atmosenv.2008.11.025, 2009. 14315, 14331

United States Department of Agriculture: Field book for describing and sampling soils, Version 2.0., Natural Resources Conservation Service, National Soil Survey Center, Lincoln, NE, available online at: <http://soils.usda.gov/technical/fieldbook/>, 2002. 14337

30 Watson, D.: The natural neighbor series manuals and source codes, *Comput. Geosci.*, 25, 463–466, doi:10.1016/S0098-3004(98)00150-2, 1999. 14321

Werczynski, S., Conen, F., Zahorowski, W., and Chambers, S.: Comparison of University of Basel and ANSTO emanometers, *Tech. rep.*, ANSTO, in preparation, 2010. 14317

## A map of radon flux at the Australian land surface

A. D. Griffiths et al.

Title Page

Abstract

Introduction

Conclusions

References

Tables

Figures

◀

▶

◀

▶

Back

Close

Full Screen / Esc

Printer-friendly Version

Interactive Discussion



- Whittlestone, S., Zahorowski, W., and Schery, S.: Radon flux variability with season and location in Tasmania, Australia, *J. Radioanal. Nucl. Chem.*, 236, 213–217, doi:10.1007/BF02386345, 1998. 14324, 14336
- Williams, A., Chambers, S., Zahorowski, W., Crawford, J., Matsumoto, K., and Uematsu, M.: Estimating the Asian radon flux density and its latitudinal gradient in winter using ground-based radon observations at Sado Island, *Tellus B*, 61, 732–746, doi:10.1111/j.1600-0889.2009.00438.x, 2009. 14315
- Zahorowski, W. and Whittlestone, S.: A Fast Portable Emanometer for Field Measurement of Radon and Thoron Flux, *Radiat. Protect. Dosim.*, 67, 109–120, 1996. 14316
- Zahorowski, W., Chambers, S., and Henderson-Sellers, A.: Ground based radon-222 observations and their application to atmospheric studies, *J. Environ. Radioact.*, 76, 3–33, doi:10.1016/j.jenvrad.2004.03.033, 2004. 14315
- Zhang, K., Wan, H., Zhang, M., and Wang, B.: Evaluation of the atmospheric transport in a GCM using radon measurements: sensitivity to cumulus convection parameterization, *Atmos. Chem. Phys.*, 8, 2811–2832, doi:10.5194/acp-8-2811-2008, 2008. 14315
- Zhuo, W., Iida, T., and Furukawa, M.: Modeling Radon Flux Density from the Earth's Surface, *J. Nucl. Sci. Tech.*, 43, 479–482, doi:10.3327/jnst.43.479, 2006. 14317
- Zhuo, W., Guo, Q., Chen, B., and Cheng, G.: Estimating the amount and distribution of radon flux density from the soil surface in China, *J. Environ. Radioact.*, 99, 1143–1148, doi:10.1016/j.jenvrad.2008.01.011, 2008. 14315, 14319, 14329, 14337

## A map of radon flux at the Australian land surface

A. D. Griffiths et al.

**Table 1.** Accumulation chamber measurements of radon flux density ordered by mean flux density.

Location	Date	Geographic extent	N <sup>a</sup>	Mean flux density mBq m <sup>-2</sup> s <sup>-1</sup>	Mean A <sub>Ra</sub> <sup>b</sup> Bq kg <sup>-1</sup>
Cataract	1998	34.2° S, 150.7° E, 7 sites within 400 m	175	12.8	16.6
Tasmania survey <sup>c</sup>	Feb, Aug 1996; Dec 1997	42.4° S, 144.9° E–40.8° S, 148.3° E	20	17.3	18.2
Goulburn	Aug 2006	35.0° S, 149.6° E–34.7° S, 149.9° E	33	18.1	17.7
Mainland survey <sup>d</sup>	Jun 1986	35.4° S, 114.5° E–12.4° S, 151.0° E	61	27.5	18.3
Goulburn	Feb 2008	35.0° S, 149.6° E–34.7° S, 149.9° E	18	51.3	19.4
Mary River	Sep 2008	12.9° S, 131.5° E–12.8° S, 131.7° E	35	185	99.2
Cowra	Feb 2008	33.9° S, 148.5° E–33.9° S, 148.6° E	24	229	82.4
Cowra	Jul 2008	34.0° S, 148.5° E–33.9° S, 148.6° E	23	264	84.1

<sup>a</sup> Number of points in data set that passed quality control and were inside radiometrics coverage area.

<sup>b</sup> Equivalent radium specific activity in topsoil, A<sub>Ra</sub>, from radiometrics. For Goulburn and Mary River these were point measurements made using a hand-held gamma spectrometer, otherwise data are taken from airborne measurements (Minty et al., 2009).

<sup>c</sup> From Whittlestone et al. (1998) (February, August 1996) and unpublished data (December 1997).

<sup>d</sup> From Schery et al. (1989).

Title Page

Abstract

Introduction

Conclusions

References

Tables

Figures

◀

▶

◀

▶

Back

Close

Full Screen / Esc

Printer-friendly Version

Interactive Discussion



## A map of radon flux at the Australian land surface

A. D. Griffiths et al.

Title Page

Abstract

Introduction

Conclusions

References

Tables

Figures

◀

▶

◀

▶

Back

Close

Full Screen / Esc

Printer-friendly Version

Interactive Discussion



**Table 2.** Emanation parameters from Zhuo et al. (2008) and grain size definitions from United States Department of Agriculture (2002). A misprint in the original table of emanation parameters has been corrected.

Soil texture	Grain Size (mm)	$f_0$	$a$	$b$	$c$
Clay	< 0.002	0.18	1.53	21.8	0.011
Silt	0.002–0.5	0.14	1.73	20.5	0.010
Sand	0.5–2	0.10	1.85	18.8	0.012

## A map of radon flux at the Australian land surface

A. D. Griffiths et al.

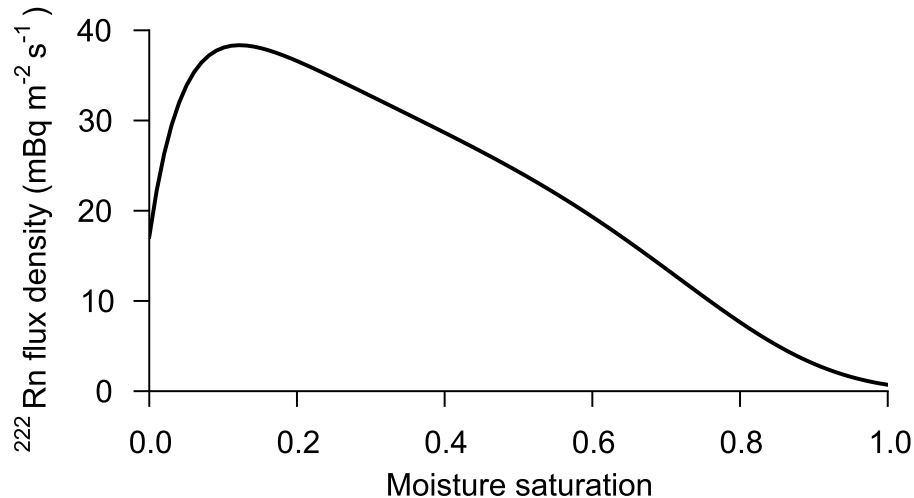


**Fig. 1.** Diffusive radon transport to the atmosphere versus soil moisture for a sandy loam (15% clay, 15% silt, 70% sand) according to Eq. (4), (5) and (6) with  $A_{\text{Ra}} = 30 \text{ Bq kg}^{-1}$ ,  $\rho_b = 1060 \text{ kg m}^{-3}$ ,  $\epsilon = 0.4$ , and  $T = 298 \text{ K}$ .

Title Page

Abstract

Introduction

Conclusions

References

Tables

Figures

◀

▶

◀

▶

Back

Close

Full Screen / Esc

Printer-friendly Version

Interactive Discussion



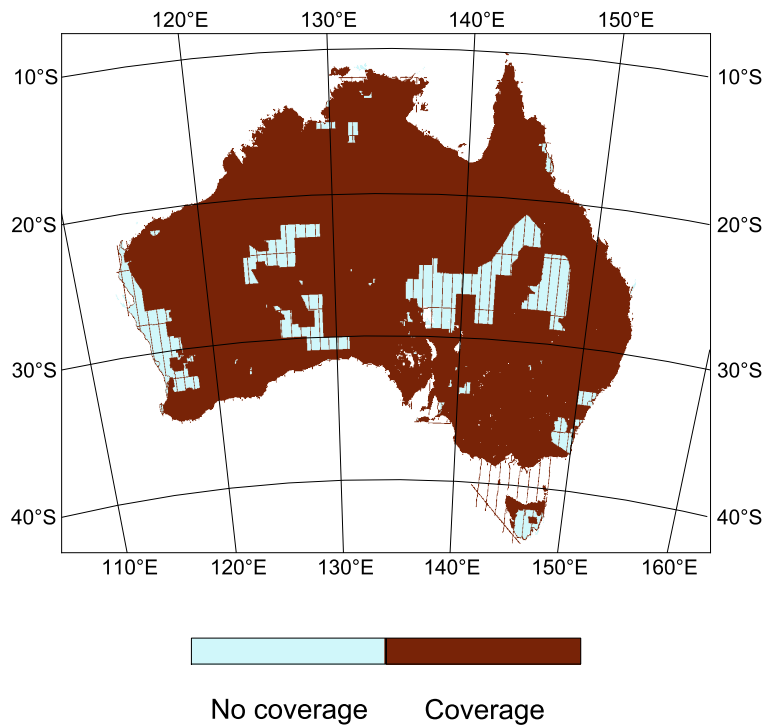


**Fig. 2.** Aerial gamma-ray survey coverage of Australia.

**A map of radon flux at the Australian land surface**

A. D. Griffiths et al.

Title Page

Abstract Introduction

Conclusions References

Tables Figures

◀ ▶

◀ ▶

Back Close

Full Screen / Esc

Printer-friendly Version

Interactive Discussion



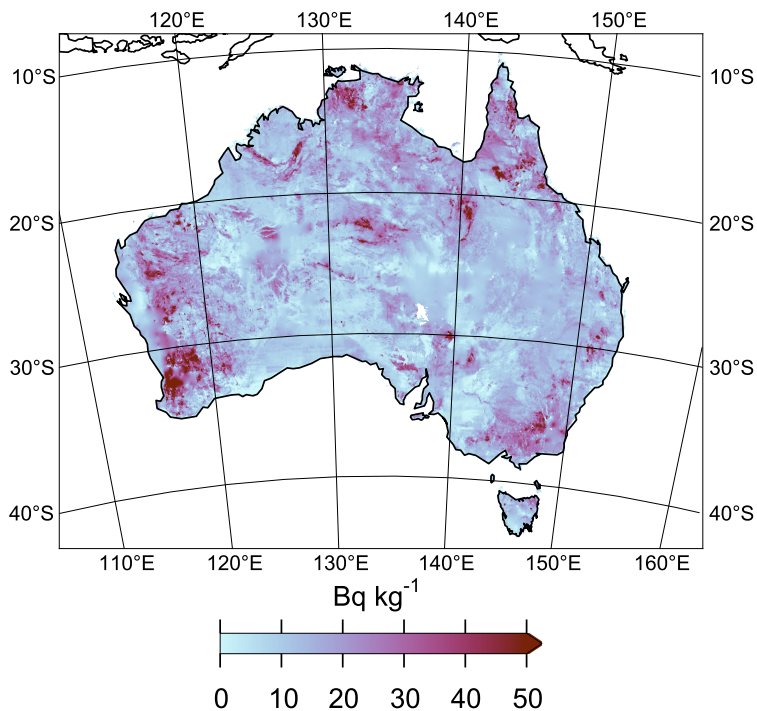


**Fig. 3.** Equivalent radium-226 specific activity in topsoil with gaps in the data filled by interpolation.

**A map of radon flux at the Australian land surface**

A. D. Griffiths et al.

Title Page

Abstract Introduction

Conclusions References

Tables Figures

◀ ▶

◀ ▶

Back Close

Full Screen / Esc

Printer-friendly Version

Interactive Discussion



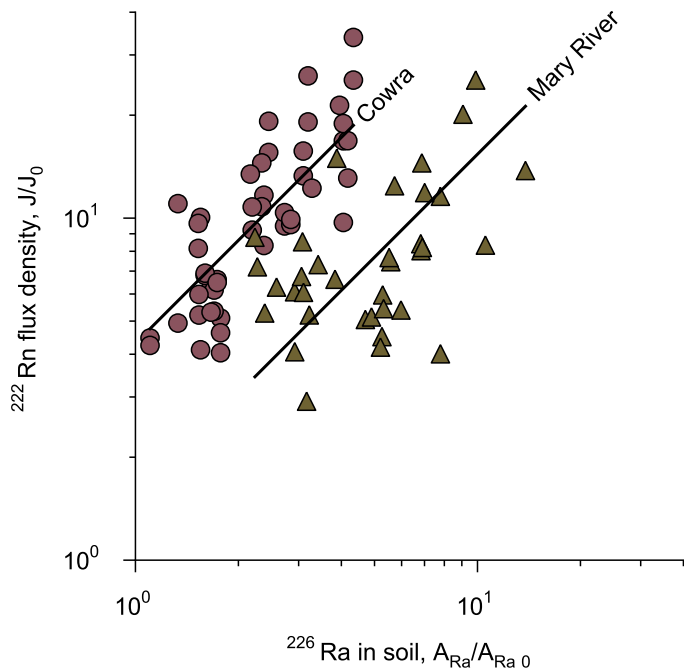


**Fig. 4.** Radon flux density versus radium–226 specific activity, as determined in the field from ground-based measurements of bismuth-214 gamma activity. The lines of best fit are  $y = 4.3x$  ( $R^2 = 0.58$ , circles mark measurements) for Cowra and  $y = 1.5x$  ( $R^2 = 0.22$ , triangles mark measurements) for Mary River. Radium activity and radon flux density are normalised by typical average values,  $A_{Ra0} = 30 \text{ Bq kg}^{-1}$  and  $J_0 = 22 \text{ mBq m}^{-2} \text{ s}^{-1}$ .

**A map of radon flux at the Australian land surface**

A. D. Griffiths et al.

Title Page	
Abstract	Introduction
Conclusions	References
Tables	Figures
◀	▶
◀	▶
Back	Close
Full Screen / Esc	
Printer-friendly Version	
Interactive Discussion	



## A map of radon flux at the Australian land surface

A. D. Griffiths et al.

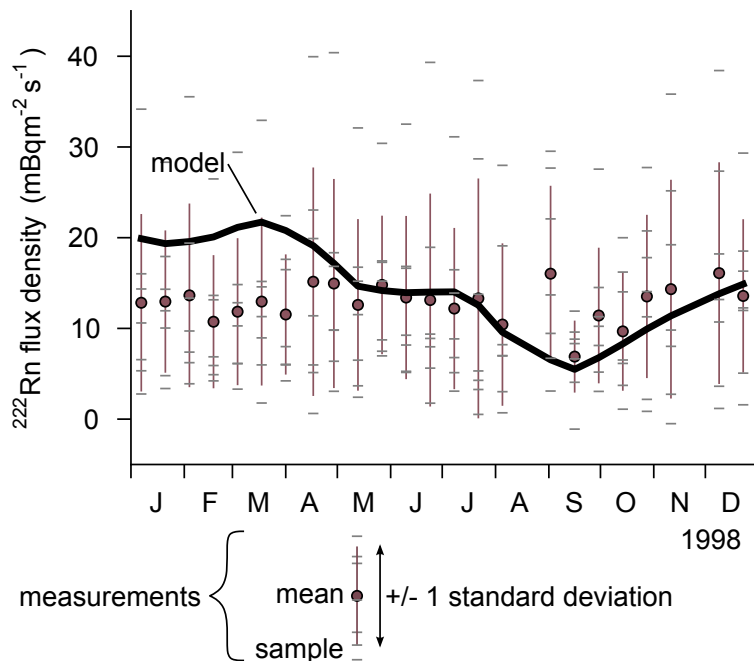


**Fig. 5.** Time series of measured and modelled radon flux density during 1998 from the Cataract data set. The average flux density over the entire year was measured to be  $12.6 \text{ mBq m}^{-2} \text{ s}^{-1}$ , whereas the uncalibrated model was  $14.5 \text{ mBq m}^{-2} \text{ s}^{-1}$ .

Title Page

Abstract

Introduction

Conclusions

References

Tables

Figures

◀

▶

◀

▶

Back

Close

Full Screen / Esc

Printer-friendly Version

Interactive Discussion



## A map of radon flux at the Australian land surface

A. D. Griffiths et al.

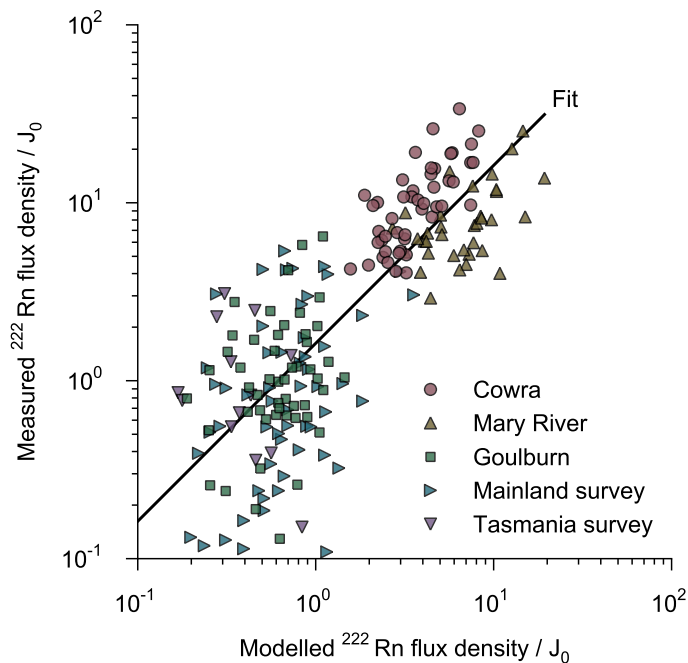


**Fig. 6.** Correlation between modelled and measured radon flux density,  $J_0 = 22 \text{ mBq m}^{-2} \text{ s}^{-1}$ . The line of best fit is  $y = 1.6x$  with  $R^2 = 0.45$ .

[Title Page](#)[Abstract](#)[Introduction](#)[Conclusions](#)[References](#)[Tables](#)[Figures](#)[◀](#)[▶](#)[◀](#)[▶](#)[Back](#)[Close](#)[Full Screen / Esc](#)[Printer-friendly Version](#)[Interactive Discussion](#)

## A map of radon flux at the Australian land surface

A. D. Griffiths et al.

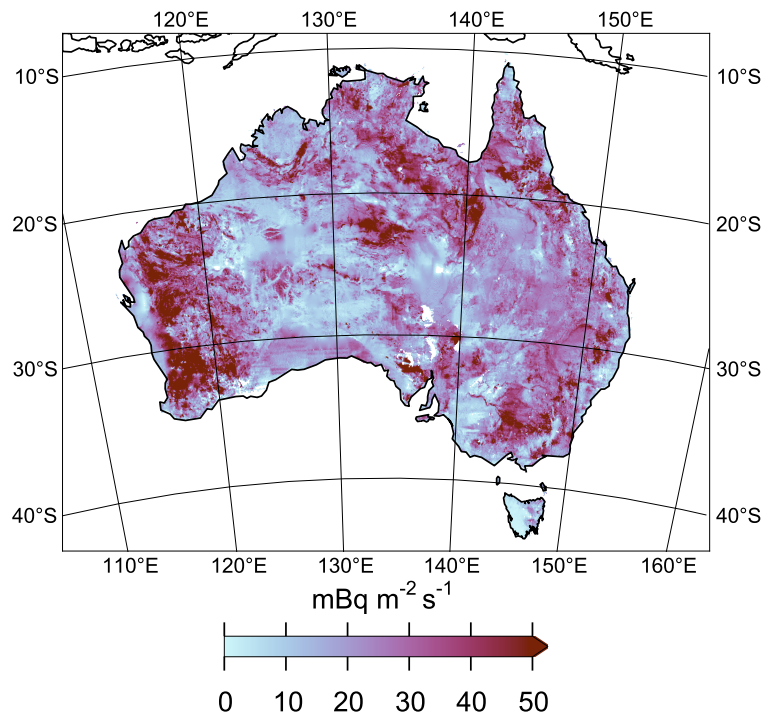


**Fig. 7.** Mean radon-222 flux density over the period 1900–2008, the area-weighted mean is  $24.1 \pm 2.2 \text{ mBq m}^{-2} \text{ s}^{-1}$ .

Title Page

Abstract

Introduction

Conclusions

References

Tables

Figures

◀

▶

◀

▶

Back

Close

Full Screen / Esc

Printer-friendly Version

Interactive Discussion



## A map of radon flux at the Australian land surface

A. D. Griffiths et al.

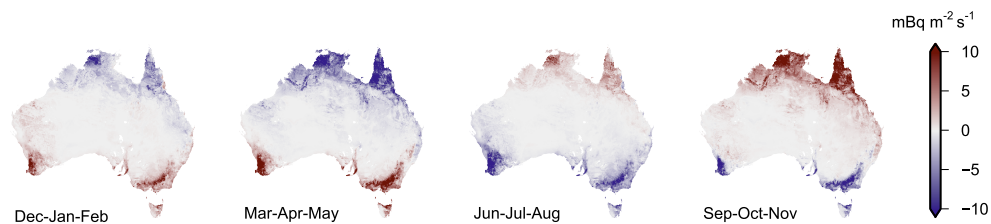


**Fig. 8.** Seasonal mean radon flux anomalies for 1900–2008.

Title Page

Abstract

Introduction

Conclusions

References

Tables

Figures

◀

▶

◀

▶

Back

Close

Full Screen / Esc

Printer-friendly Version

Interactive Discussion



## A map of radon flux at the Australian land surface

A. D. Griffiths et al.

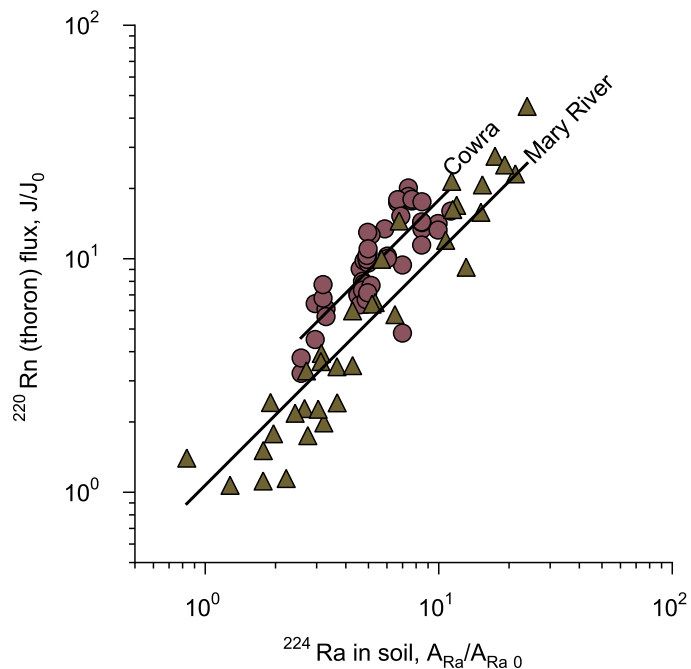


**Fig. 9.** Observed correlation between radium-224 specific activity, as determined from field radiometrics using the thorium channel, and radon-220 (thoron) flux. The lines of best fit are  $y = 1.8x$  ( $R^2 = 0.55$ , circles mark measurements) for Cowra and  $y = 1.1x$  ( $R^2 = 0.79$ , triangles mark measurements) for Mary River. Radium-224 activity is normalised by  $A_{\text{Ra}0} = 30 \text{ Bq kg}^{-1}$  and flux by  $J_0 = 1.7 \text{ Bq m}^2 \text{ s}^{-1}$ .

Title Page

Abstract

Introduction

Conclusions

References

Tables

Figures

◀

▶

◀

▶

Back

Close

Full Screen / Esc

Printer-friendly Version

Interactive Discussion

